DOI: 10.1002/ejic.200900603

Polyoxometalates in Polyelectrolyte Multilayer Films: Direct Loading of $[H_7P_8W_{48}O_{184}]^{33-}$ vs. Diffusion into the Film

Vincent Ball,*[a,b] Falk Bernsmann,[a,b] Sandra Werner,[a,b] Jean-Claude Voegel,[a,b] Luis Fernando Piedra-Garza,[c] and Ulrich Kortz[c]

Keywords: Polyoxometalates / Polyelectrolyte multilayer films / Electrochemistry

The immobilization of polyoxometalates (POMs) into thin organized films is of major importance for the development of functional devices like electrochromic films and catalysts. We investigate herein two methods to incorporate the wheel-shaped tungstophosphate $[H_7P_8W_{48}O_{184}]^{33-}$ (P_8W_{48}) polyoxometalates (POM) into polyelectrolyte multilayer (PEM) films, which offer the advantage of controlled thickness and ease of processability. The first method, whose feasibility has been widely demonstrated, consists in the alternate deposition of a polycation and the negatively charged POM. The second method has never been used to load POMs into thin films: an exponentially grown polyelectrolyte multilayer film, made from sodium hyaluronate (HA) and poly-L-lysine (PLL), is brought in contact with the POM solution to allow its passive diffusion into the PEM film. Both methods of incorporation are compared in terms of effective POM concentration in the film. In addition it is shown that the second method leads to a maximum in the amount of incorporated POM as a function of its concentration in solution.

Introduction

Polyoxometalates (POMs) are known since 1826 and systematically synthesized for almost a century[1,2] Research on this compound class becomes an increasingly popular subdomain of supramolecular chemistry[3] because they are obtained through the non-covalent association of metal oxide fragments. They find very interesting applications in catalysis,[4] electrooptical devices[5] and last but not least in medicine for their potential applications.[6–10] Related to potential applications in both medicine and surface science, their surface chemistry is being more and more investigated.[11] Different immobilization methods of POMs on solid surfaces have been demonstrated: chemisorption on carbon or metallic surfaces,[11] Langmuir Blodgett deposition,[12] electrodeposition[13] and deposition using the concept of layer-by-layer (LBL) assembly of oppositely charged species.[14] This method relies basically on the charge overcompensation after the adsorption of a multicharged species at a solid-liquid interface[15] and offers the advantage of a great versatility: it can be applied on any kind of charged surfaces even on small colloids,[16] it does not need specific equipment and it can be automated. In addition, films can be deposited by spraying[17] or spin casting[18] to speed up the deposition. Several reviews describe the fundamental concepts as well as the applications of PEMs produced by the LBL method.[19,20] The field of surface coating with PEMs has found great success to design drug delivery systems on micro and nanoparticles.[21] Many films have been produced incorporating nanoparticles and among these studies are some using POMs as the inorganic building block.[22–28] The possible application of POM-containing PEM films as electrochromic and photochromic materials has already been demonstrated.[23e,28] Wheel shaped POMs like $[H_7P_8W_{48}O_{184}]^{33-}$ may have very interesting electrocatalytic properties[29] as well as electrochromic properties. This is the reason why we want to investigate them on surfaces. The advantage of LBL deposition is that the amount of active molecules can be controlled through the number of deposition steps: in most situations the amount of active molecules is proportional to the number of layer pairs, where one layer pair is obtained by the deposition of one polycation and one polyanion layer. However, these linearly growing films have to be permeable to the molecules that should undergo a chemical reaction in contact with the catalytical centres embedded in the film. This is however not always the case, particularly in the case of ions.[30] From this point of view, PEM films whose thickness grows exponentially with the number of deposition steps[31] are very promising owing to their permeability to ions[32] and even to charged colloidal nanoparticles.[33] It has recently been

[a] Institut National de la Santé et de la Recherche Médicale, Unité 977,
11 rue Humann, 67085 Strasbourg Cedex, France
Fax: +33-3-90243379
E-mail: vincent.ball@medecine.u-strasbg.fr
[b] Faculté de Chirurgie Dentaire, Université de Strasbourg,
1 Place de l'Hôpital, 67000 Strasbourg, France
[c] School of Engineering and Science, Jacobs University Bremen,
P. O. Box 750561, 28725 Bremen, Germany

Supporting information for this article is available on the WWW under http://dx.doi.org/10.1002/ejic.200900603.

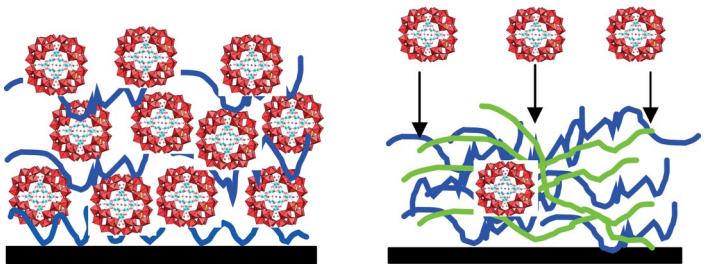

Scheme 1. Representation of the two methods used to load P_8W_{48} into PEM films. On the left, method I consists on the alternated adsorption of PLL and the POM, whereas on the right the POMs are allowed to diffuse into $(PLL\text{-}HA)_n$ multilayer films.

demonstrated that CdTe quantum dots capped with thioglycolic acid are able to diffuse in PEM films made from poly(acrylic acid) (PAA) and poly(diallyldimethyl ammonium chloride) (PDADMA).[33] Even if these PEMs were several tens of μm thick, confocal laser scanning microscopy (CLSM) showed that the filling of the film was homogeneous and thermogravimetric analysis showed that the mass fraction of CdTe can reach 20–22%.[33] It is hence the aim of this investigation to build up linearly growing PEM films from poly-L-lysine (PLL) and from Na_{33} $[H_7P_8W_{48}O_{184}]\cdot 92H_2O$ (loading method I) and to compare the concentration of POM in these architectures with the concentration that can be reached when an exponentially growing film made from sodium hyaluronate (HA) and PLL is put in contact with a solution of $Na_{33}H_7[P_8W_{48}O_{184}]\cdot 92H_2O$ at various concentrations (loading method II). It has been demonstrated that the thickness of PEM films made from HA and PLL increases exponentially with the number of deposited layer pairs in the presence of 0.15 M NaCl and at pH 5–6.[31a,31b] A film obtained by the deposition of n pairs of PLL and HA will be denoted $(PLL\text{-}HA)_n$. The difference in the two loading methods is depicted in Scheme 1.

When using UV visible spectroscopy (UV/Vis) and cyclic voltammetry (CV) we found that the POM concentration obtained by method II is similar to that observed with method I and that the diffusion kinetics is extremely slow (characteristic times of the order of a few hours). However, the POMs present in the films loaded by method II do not desorb when the films are brought in contact with buffer solution. A very interesting finding is that the POM concentration in the $(PLL\text{-}HA)_n$ film is not a monotonous function of the bulk concentration used to load the film. Nevertheless combination of UV/Vis and CV suggests that the films are homogeneously filled with POM by loading method II at all the investigated concentrations. In the following we will denote the used POM with the shorthand notation P_8W_{48} making abstraction of the Na^+ counterions.

Results and Discussion

We used quartz crystal microbalance with monitoring of the dissipation (QCM-D) to investigate the time needed to reach saturation adsorption in both the deposition of PLL and P_8W_{48} (Figure 1, A). It appears that saturation in the adsorbed amounts are reached in less than 5 min and that P_8W_{48} does not desorb when it is put in contact with either the sodium acetate buffer or the PLL solution (at 0.7 g/L). This finding is in contrast with the observed partial desorption of the adsorbed $(NH_4)_{42}[(H_2O)_n \subset Mo_{132}O_{372}(CH_3COO)_{30}(H_2O)_{72}]$ when the film is put in contact with a solution containing poly(allylamine hydrochloride).[23b] Hence in the following, a deposition time of 5 min was used

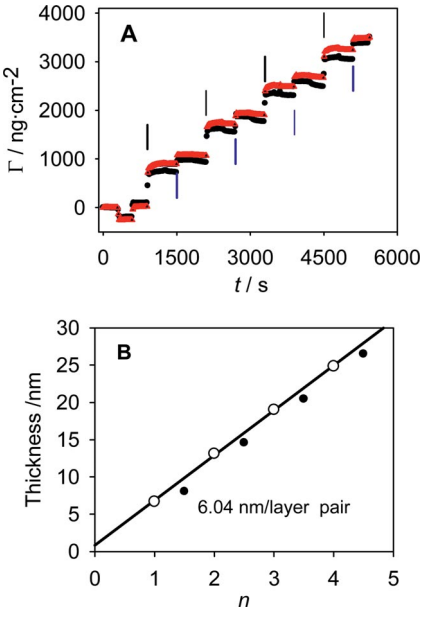

Figure 1. **A**: QCM-D experiment displaying the build up of a PEI-$(P_8W_{48}\text{-}PLL)_n$ film. The concentration of P_8W_{48} and of PLL are of 2.4×10^{-5} and 2.5×10^{-3} mol L^{-1}, respectively, in 10 mM sodium acetate + 150 mM NaCl buffer at pH 4.0. The concentration of PLL is expressed in mol of lysine monomers. The black vertical lines and blue vertical lines correspond to the injection of P_8W_{48} and PLL, respectively. The injection of PEI (at t = 5 min) has not been labelled. Data calculated from the third harmonic (black line, ν ca. 15 MHz) and from the fifth harmonic (red line, $\nu \approx 25$ MHz) **B**: evolution of the thickness of the deposit, calculated from the Sauerbrey relationship, as a function of the number of deposited layer pairs. The deposition of P_8W_{48} (open cirlce) corresponds to the end of a layer pair, whereas the deposition of PLL (filled circle) marks the beginning of a layer pair. The straight line corresponds to a linear regression to the thickness evolution at the end of each layer pair.

for the deposition of each layer of a PEI-(P_8W_{48}-PLL)$_n$ film where poly(ethylene imine) (PEI) was used as anchoring layer to the silicon oxide substrate. The reduced frequency changes for the first, third, fifth and seventh overtone of the QCM-D signal being identical (within the experimental precision) we used the QCM-D frequency changes to calculate the film thickness according to: $d = \Gamma/\rho$, where Γ is the mass surface coverage obtained from the experimental data using the Sauerbrey equation[34] and ρ is the density of the film, which we set arbitrarily equal to 1.3 g cm^{-3}.

Anyway, the QCM-D frequency change does not only take the mass of PLL and P_8W_{48} into account but also that of the water of hydration. Figure 1 (B) shows that most of the thickness increase is due to the deposition of the POM. In addition the average thickness increment due to the deposition of each P_8W_{48} layer is of (4.6 ± 0.4) nm, whereas the PLL layers are much thinner, on average (1.5 ± 0.2) nm. The thickness increment of each P_8W_{48} layer is thus much larger than expected on the basis of the radius deduced from the X-ray crystal structure (2.2 nm).[35] At this level we can attribute this finding to either an aggregation of the POM upon its adsorption on a PLL ending film or to the effect of hydration contributing to an increase in the apparent layer thickness.

AFM height measurement (Figure 2) of the dried film from a scratched PEI-(P_8W_{48}-PLL)$_4$ deposit show that a film is already formed for such a low number of deposition steps: indeed, in the non-scratched region, the silicon oxide surface is totally covered with the PEM. In addition the step height between the film surface and the scratched region is between 25 and 35 nm with a root mean squared roughness of about 10 nm.

The average thickness obtained by AFM is compatible with the thickness calculated from QCM-D where the thickness increment per layer pair is of (6.1 ± 0.6) nm. This later value is larger than, but not inconsistent with the thickness increment obtained from single wavelength ellipsometry, namely (3.25 ± 0.1) nm (Figure 1 of the Supporting Information). This trend is in line with other comparisons between film thicknesses estimated from piezoelectric and optical sensors.[36] It has to be noted that the thickness determined by ellipsometry is probably overestimated by the fact that the refractive index of the film was arbitrarily fixed at 1.465 (See experimental section).

To get a better picture of the film deposition process, we used UV/Vis spectroscopy and CV to calculate the molar surface coverage of the POM in the films. The data from both kinds of experiments are displayed in Figures 3 and 4 respectively. As for the QCM-D (Figure 1) and the ellipsometry data (Figure 1 of Supporting Information), the UV/Vis experiments demonstrate that the amount of deposited material increases linearly with the number of layer pairs. In addition the film is transparent at wavelengths higher than 400 nm demonstrating that the film is not scattering

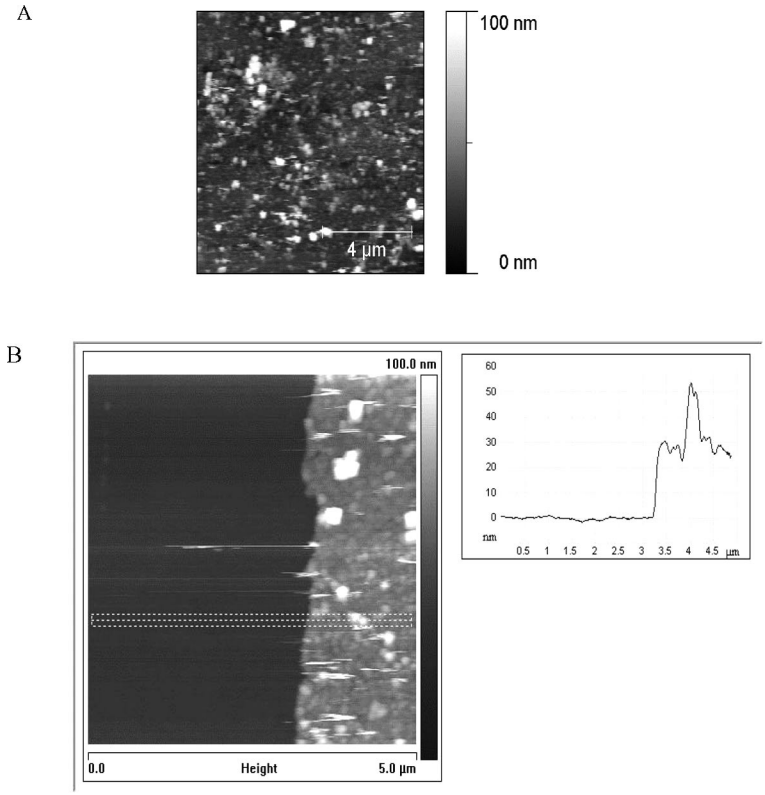

Figure 2. **A**: AFM topography of a PEI-(P_8W_{48}-PLL)$_4$ film deposited on the surface of the quartz crystal used for the QCM-D experiment (Figure 1). **B**, left: topography of the same film close to a needle scratched region. **B**, right: average step profile in the dashed rectangles represented on the left.

light and hence that it does not contain large in homogeneities at the scale of the wavelength of the beam used in the spectroscopy experiments The increment in absorbance per layer pair is of 0.054 and 0.033 at wavelengths of 226 and 250 nm respectively.

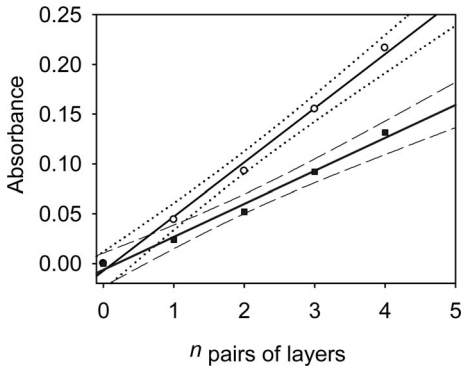

Figure 3. Evolution of the absorbance of PEI–$(P_8W_{48}$-PLL$)_n$ films as a function of the number of deposited layer pairs at 226 nm (open circle) and at 250 nm (black filled square). The thick lines correspond to a linear regression to the data whereas the dashed lines correspond to the limit of the 95% confidence intervals.

To estimate the molar surface coverage per layer of deposited P_8W_{48}, Γ_{UV}, we can only use the absorbance at 250 nm because PLL, the other component of the film is absorbing light up to 230 nm. The Beer–Lambert law allows calculating, Γ_{UV}, directly from the absorbance increment A_{UV} per bilayer, according to Equation (1).[23b,23d]

$$\Gamma_{UV} = \frac{A_{250}}{2 \cdot \varepsilon_{250}} \quad (1)$$

where the factor 2 accounts for the fact that the film is covering both sides of the quartz slide. The extinction coefficient of P_8W_{48} in the sodium acetate buffer at pH 4.0 was calculated from a calibration plot using P_8W_{48} dissolved at different concentrations: $\varepsilon_{250} = 2.01 \times 10^5$ L mol^{-1} cm^{-1} = 2.01×10^8 cm^2 mol^{-1} (the molecular mass of the POM is equal to 14446 g mol^{-1}). The area occupied per molecule, S_{UV}, can be easily obtained from Γ_{UV}, we obtain $\Gamma_{UV} = (8.2 \pm 0.5) \times 10^{-11}$ mol cm^{-2} and S_{UV} = 2.0 nm^2. The surface occupied per POM cluster is clearly lower that the 3.8 nm^2 expected on the basis of a disk 1.1 nm in radius according to the crystal structure of P_8W_{48}.[35] This strongly suggests that that POM adsorbs as small aggregates and at least as more than a single monolayer on a PLL ending deposit. Such a finding has been already described by the group of Kunitake in the case of ammonium octamolybdate deposited in PEM films containing poly(allylamine) (PAH) as a polycation.[22]

To confirm this observation as well as to check the electrical connectivity between the POMs in the PEI-$(P_8W_{48}$-PLL$)_n$ architecture we performed cyclic voltammetry measurements. These experiments were performed on amorphous carbon working electrodes, hence on a different substrate as those used in the previously described characterization methods. In the case where the POMs are immobilized in the PEI-$(P_8W_{48}$-PLL$)_n$ films, the difference in the peak potential between A1 and C1 never exceeds 25–30 mV for n values between 1 and 8 (Figure 4, B) and the oxidation and reduction peak currents for a given number of layer pairs scale linearly with the potential scan rate, which is a signature of a thin-film behaviour (Figure 2 of the Supporting Information). This contrasts with the CV of P_8W_{48} in solution where the oxidation peak A1 and its corresponding reduction peak C1 are separated by 80 mV (at a scan rate of 50 mV s^{-1}). In addition, for experiments performed in solution, the oxidation and reduction peak currents scaled as the square root of the scan rate, i.e. their electrochemistry is limited by the diffusion from the solution to the electrode surface (data not shown). It also appears from Figure 4 (A), that the oxidation and reduction peak intensity increases linearly with the number of deposited layer pairs in the PEI-$(P_8W_{48}$-PLL$)_n$ films. Each layer pair contributes to $i_p = (2.25 \pm 0.02) \times 10^{-7}$ A, as obtained from experiments performed at a scan rate of 10 mV s^{-1}.

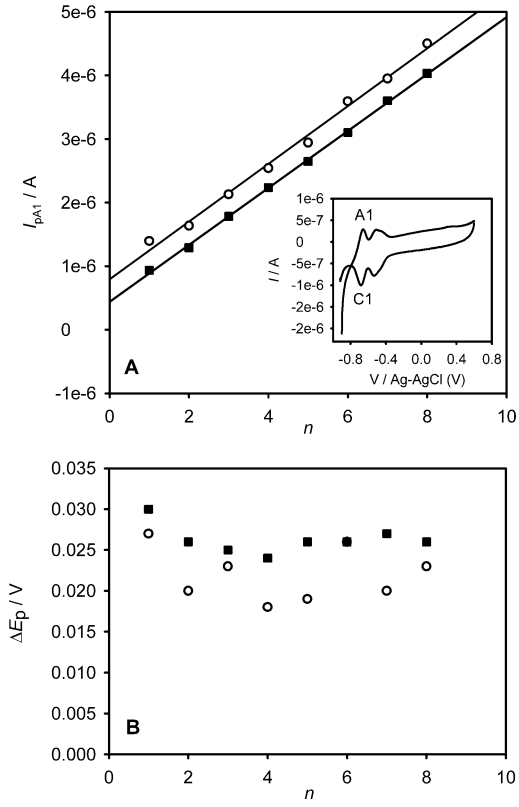

Figure 4. **A**: Evolution of the peak current I_{pA1} of the first oxidation peak of P_8W_{48} in PEI-$(P_8W_{48}$-PLL$)_n$ films as a function of n in two independent experiments. The measurements were performed at a scan rate of 10 mV s^{-1}. Inset: cyclic voltammogram of a PEI-$(P_8W_{48}$-PLL$)_2$ film at a scan rate of 10 mV s^{-1}. A1 and C1 denote the first oxidation and reduction peak of P_8W_{48} in the film. **B**: Peak separation ΔE_p between A1 and C1 as a function of n. The CV measurements were performed at a scan rate of 10 mV s^{-1} in two sets of independent experiments.

This value allows calculating the surface coverage, Γ_{volta}, based on the cyclic voltammetry experiments, see Equation (2).[37]

$$\Gamma_{volta} = \frac{i_p \cdot R \cdot T\left(4 - 2 \cdot \gamma \cdot \Gamma_{volta}\right)}{n^2 \cdot F^2 \cdot \upsilon \cdot A} \quad (2)$$

i_p, R, T, n, F, υ are the peak current intensity increment per layer pair, the gas constant, the absolute temperature, the number of electrons implied in the A1-C1 redox process (here $n = 2$), Faraday's constant and the potential scan rate, respectively. A is the area of the electrode and γ is an interaction term of the redox probe with the matrix of the film. In the case where γ is very small, which should be the case here because i_p scales linearly with υ, equation (2) simplifies to Equation (3).

$$\Gamma_{volta} = \frac{4 \cdot R \cdot T \cdot i_p}{n^2 \cdot F^2 \cdot \nu \cdot A} \quad (3)$$

From the value of i_p we obtain a surface coverage of $\Gamma_{\text{volta}} = (1.92 \pm 0.2) \times 10^{-10}$ mol cm^{-2} per layer and a corresponding area per P_8W_{48} of about 0.9 nm^2. The surface coverage obtained by electrochemistry in this study is of the same order of magnitude as the value obtained by Volkmer et al., namely 1.3 or 1.7×10^{-10} mol cm^{-2} for Eu(H_2O)-$[P_5W_{30}O_{110}]^{12-}$ POM depending on the layering structure of the POM with the used polycation, PAH.[23d] It has to be noted that Γ_{UV} and Γ_{volta} are very close (within a factor of about 2). The difference between the surface coverage calculated from the UV/Vis and the CV data may mainly originate from the non-validity of two assumptions: (i) we assumed that the interaction term γ in equation (2) is equal to zero, (ii) and that the electrochemical area of the electrode, A, is equal to its projected area, hence neglecting the surface roughness which is different from zero owing to the fact that the electrode was polished with a 50 nm alumina suspension before each experiment (see Experimental section). From the electrochemistry data as well from the thickness increment per bilayer, obtained by QCM-D, we can calculate the loading efficiency (defined as the current per layer pair divided by the corresponding thickness) of the PEM film loaded with P_8W_{48} according to method I, it amounts to 37.4×10^{-9} A nm^{-1}. To obtain this value, we used the thickness calculated from the QCM-D experiment because it corresponds to an hydrated film.

We will now investigate the loading of PEI-(PLL-HA)$_n$ PEM films with P_8W_{48} from the solution in contact with the as-built film (Scheme 1). As a first control we investigated the film stability when it is put in contact with a buffer solution containing P_8W_{48} by means of attenuated total reflection Fourier-transfom infrared spectroscopy (ATR-FTIR). To that aim we deposited a PEI-(HA-PLL)$_{12}$-HA film on the ZnSe crystal. The thickness of this film is significantly higher than the wavelength-dependant penetration depth of the evanescent wave into the solution (about 1 μm at 1000 cm^{-1}) as shown by the fact that the signal of the amide I band characteristic of PLL does not increase significantly after the deposition of the 9th HA-PLL layer pair (Figure 3 of the Supporting Information). When such a film is put in contact with a P_8W_{48}-containing buffer, the characteristic vibration peaks of the POM (at 704, 793 and 917 cm^{-1}) appear in the region sensed by the evanescent wave even after only 2 h of contact between the film and the solution (Figure 5). The amide I band intensity, attributed to PLL increases during the infiltration of the POM in the PEM film, which means that at least in the region of the film close to the ZnSe crystal, the film undergoes some deswelling, i.e. an increase in the polyelectrolyte concentration. It also appears in Figure 5 that the intensity of the peaks attributed to P_8W_{48} is higher when the film is put in contact with a P_8W_{48} solution at 1.2×10^{-5} M than with a solution at 1.2×10^{-4} M. In all cases the peak positions are identical to those of the POM in solution at 1.2×10^{-4} M, meaning that P_8W_{48} keeps its integrity when incorporated in the PEM film. In addition, the peak intensity of P_8W_{48} in the film is always higher than in the corresponding solution (Figure 5 displays the spectrum of P_8W_{48} in the film when it is loaded from a solution at 1.2×10^{-4} M as well as its spectrum in solution at the same concentration). This finding means that the PEM film allows to concentrate the POM. This result is qualitatively similar to that obtained for negatively charged CdTe quantum dots diffusing in PEM films made from PAA and PDADMA.[33]

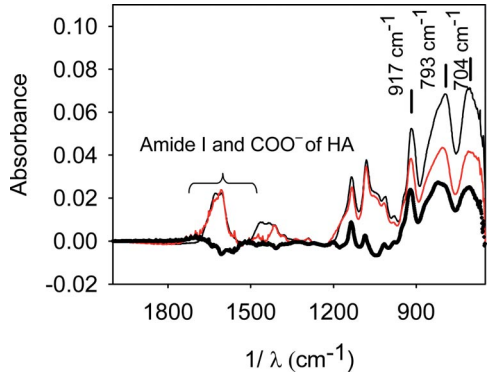

Figure 5. ATR infrared spectrum of two PEI-(HA-PLL)$_{12}$-HA films put in contact during 2 h with a P_8W_{48} containing solution having a concentration of 1.2×10^{-5} M (black line) and 1.2×10^{-4} M (red line). The POM solution was removed from the flow cell before spectral acquisition and the absorbance was calculated with respect to that of the PEI-(HA-PLL)$_{12}$-HA film (Figure 3 of the Supporting Information). The spectra were also compared to that of a P_8W_{48} solution at 1.2×10^{-4} M flowing atop the ZnSe crystal (bold black line).

Nevertheless the ATR configuration of the IR measurement makes a quantitative determination of the POM concentration in the film very difficult. Hence we again used CV and UV/Vis spectroscopy to investigate both the permeation kinetics as well as the concentration of P_8W_{48} in the PEI-(HA-PLL)$_n$-HA films (in this study we restricted the measurements to films ending with a negatively charged layer, having hence a negative surface potential which constitutes a priori a barrier for the negatively charged POM).

UV/Vis spectroscopy (Figure 6) as well as CV (Figure 7) show that the permeation kinetics as well as the steady state concentration of P_8W_{48} in the PEI-(HA-PLL)$_9$-HA films are concentration dependant, as anticipated from the ATR-FTIR experiments. In addition, the permeation kinetics are extremely slow, the time needed to reach saturation lying in the 1–25 h time interval depending on the solution concentration of P_8W_{48}. This characteristic time τ was determined by fitting equation (4) to the experimental CV data.

$$i_p(t) = i_{p,\max} \cdot \left(1 - \exp\left(\frac{-t}{\tau}\right)\right) \quad (4)$$

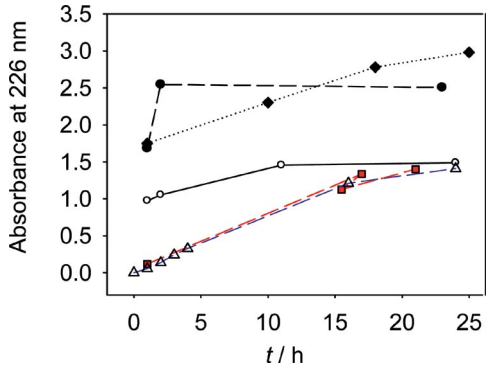

Figure 6. Permeation kinetics of P_8W_{48} in PEI-(HA-PLL)$_9$-HA films as followed by UV/Vis spectroscopy as a function of the concentration in POM: open triangle 1.2×10^{-6} M, red filled square 2.4×10^{-6} M, filled circle 1.2×10^{-5} M, filled diamond 2.4×10^{-5} M, open circle 1.2×10^{-4} M. The lines are only aimed to guide the eye.

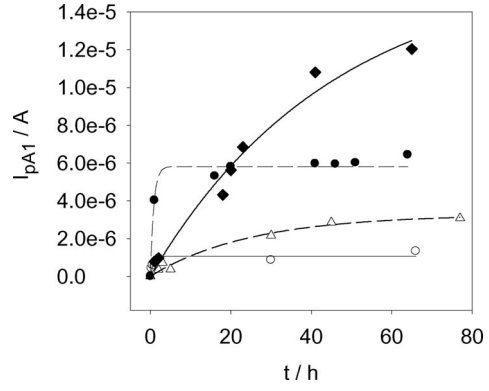

Figure 7. Permeation kinetics of P_8W_{48} in PEI-(HA-PLL)$_9$-HA films as followed by CV for different concentrations in POM: open triangle: 1.2×10^{-6} M, filled circle 1.2×10^{-5} M, filled diamond 2.4×10^{-5} M,(open circle) 1.2×10^{-4} M. I_{pA1} represents the first oxidation peak current of P_8W_{48} as a function of time t (see inset of Figure 4a). All the data were acquired at a scan rate of 10 mV s^{-1}. The lines correspond to the fit of equation (4) to the data.

The quality of the fits was satisfactory but not excellent as can be seen in Figure 7, hence the value of the characteristic time is only given as an indication (Table 1).

The data from the UV/Vis and CV experiments are in qualitative agreement in the sense that the amount of incorporated POM is maximal at a bulk concentration of about 10^{-5} M. It has to be noted that by UV/Vis one detects the optical effect of all the POMs present on both sides of the quartz slide (saturation of the detector was not reached) whereas CV may only be sensitive to the POM in close contact with the working electrode.

Table 1. Influence of the bulk concentration in P_8W_{48} on the oxidation current of peak A1 for loading methods I and II.

Loading method	C [a] [mol L^{-1}]	τ [b] [h]	I_{pA1} [c] [A]
II	1.2×10^{-6}	25	3.08×10^{-6}
II	1.2×10^{-5}	0.9	6.44×10^{-6}
II	2.4×10^{-5}	18	1.18×10^{-5}
II	1.2×10^{-4}	0.8	1.33×10^{-6}
I	2.4×10^{-5}	no kinetic effect	$(2.25\pm0.02)\times10^{-7}$

[a] Concentration of the P_8W_{48} solution in contact with the PEI-(HA-PLL)$_9$-HA film in the case of loading method II or of the solution used to build up the PEI-(P_8W_{48}-PLL)$_n$ films in the case of loading method I. [b] Characteristic time of the filling process of PEI-(HA-PLL)$_9$-HA films determined by fitting equation (4) to the experimental CV data. This fit is only meaningful in the case of loading method II. [c] Intensity of the oxidation peak A1 at the end of the filling process in case where the P_8W_{48} loading is performed according to method II. In the case of method I the given value corresponds to the oxidation current increment per layer pair, as obtained from Figure 4 (A).

However, if a percolation threshold in the incorporated amount of P_8W_{48} is reached, the measured current may be an indication of the whole amount of incorporated POM, as has been shown in the case of method I. At first glance the occurrence of a maximum in the amount of P_8W_{48} incorporated in the PEI-(HA-PLL)$_9$-HA films is surprising. One could provide a first explanation for this effect: when the solution concentration increases, the rate of permeation increases too, as suggested by the decrease in the characteristic filling time (Table 1), producing a barrier at the topmost part of the PEM film. This barrier could impede the POMs to reach the lower part of the PEM film. If this filling mechanism would occur, the CV and UV/Vis data will not be in direct correlation, owing to the fact that in the case where a barrier is formed the electrode will not necessarily be able to oxidize/reduce all the present P_8W_{48}anions. However if we plot the absorbance at 226 nm at the end of the permeation kinetics (Figure 6) as a function of the oxidation current of peak A1 at saturation (Table 1), we see that both methods used to determine the film filling provide data that are in linear correlation (Figure 8). This excludes the validity of a barrier mechanism to explain the reduction in the amount of loaded POM at concentrations higher than 10^{-5} mol L^{-1} and suggests that the films are always homogeneously filled with POMs at the saturation of the filling kinetics.

At this level, there is no reasonable assumption for the non-monotonous filling of the PEM films with P_8W_{48} as a function of its solution concentration. It is nevertheless a reproducible phenomenon as shown by the data from independent experiments performed with different characterization techniques [ATR-FTIR spectroscopy (Figure 5), UV/Vis spectroscopy (Figure 6) and CV (Figure 7)]. From Table 1 one sees that the maximal current of peak A1 (equal

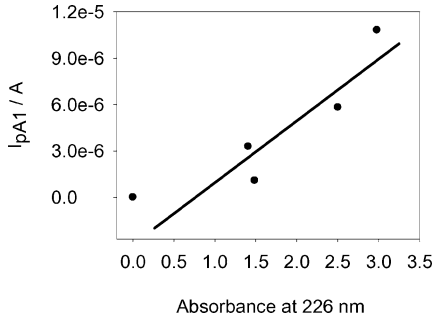

Figure 8. Relationship between the oxidation current I_{pA1} corresponding to peak A1 (Figure 7) and the absorbance at 226 nm at the end of the loading kinetics (Figure 6) of P_8W_{48} in PEI-(HA-PLL)$_9$-HA PEM films. The thick line does not correspond to a fit, it is meant to guide the eye.

to the corresponding reduction current of peak C1) is pretty much higher, by at least an order of magnitude to the maximal current per layer pair obtained when P_8W_{48} is deposited according to method I. However, the PEI-(HA-PLL)$_9$-HA film is much thicker (about 1 μm measured by confocal laser scanning microscopy) than the PEI-(P_8W_{48}-PLL)$_8$ films (about 50 nm obtained from the QCM-D experiment). Hence to make a better comparison between the two loading methods, we also calculated the loading efficiency obtained when the POMs are infiltrated in the P_8W_{48} films according to method II. At the bulk concentration of 2.4×10^{-5} M, method II yields a loading efficiency of 10.8×10^{-9} A nm^{-1}. Method I allows to reach a loading efficiency of 37.4×10^{-9} A nm^{-1}, being only slightly more advantageous in terms of loading efficiency, by a factor of about 3–4. It has to be noted that our comparison is only semi-quantitative because we neglected the swelling that the POM causes upon its diffusion into the PEI-(HA-PLL)$_9$-HA film in the calculation of the film thickness. After 2 h of loading we observed that (PLL-HA)$_{30}$-PLL(FITC) films, labelled with PLL(FITC) swelled by a factor of about 2 (Figure 4 of the Supporting Information) when put in contact with P_8W_{48} at 6×10^{-5} M. The film swelling was measured by means of confocal laser scanning microscopy (CLSM). At all the other concentrations the film swelling was much smaller, suggesting that the maximum load in POM, also found at around 10^{-5} M, is related to the maximum swelling ability of the film. We will investigate the swelling kinetics of the PLL-HA films in contact with P_8W_{48} solutions for prolonged time durations by means of CLSM in a forthcoming investigation. CLSM shows that the PLL-HA films are extremely smooth as long as the number of layer pairs is higher than 10[31a,31b] however, the incorporation of P_8W_{48} increases the film roughness to the 50–100 nm range but without modifying the transparency of the films. Indeed if the film roughness would be of the order of the wavelength of visible light, it would not remain transparent above the absorption band of P_8W_{48} ie above 320 nm (Figure 5 of the Supporting Information) We did not use AFM to image the (PLL-HA)$_{30}$-PLL(FITC) films owing to their viscous liquid state[40] which makes AFM imaging very tedious. CLSM also highlighted an intriguing self assembly processes of the POMs: they seem to be highly aggregated at the surface of the (PLL-HA)$_{30}$-PLL(FITC) PEM film after two hours of contact with a P_8W_{48} solution at 1.2×10^{-4} mol L^{-1} (Figure 9). The film appears to be covered with star like structures of about 20–30 μm in diameter.

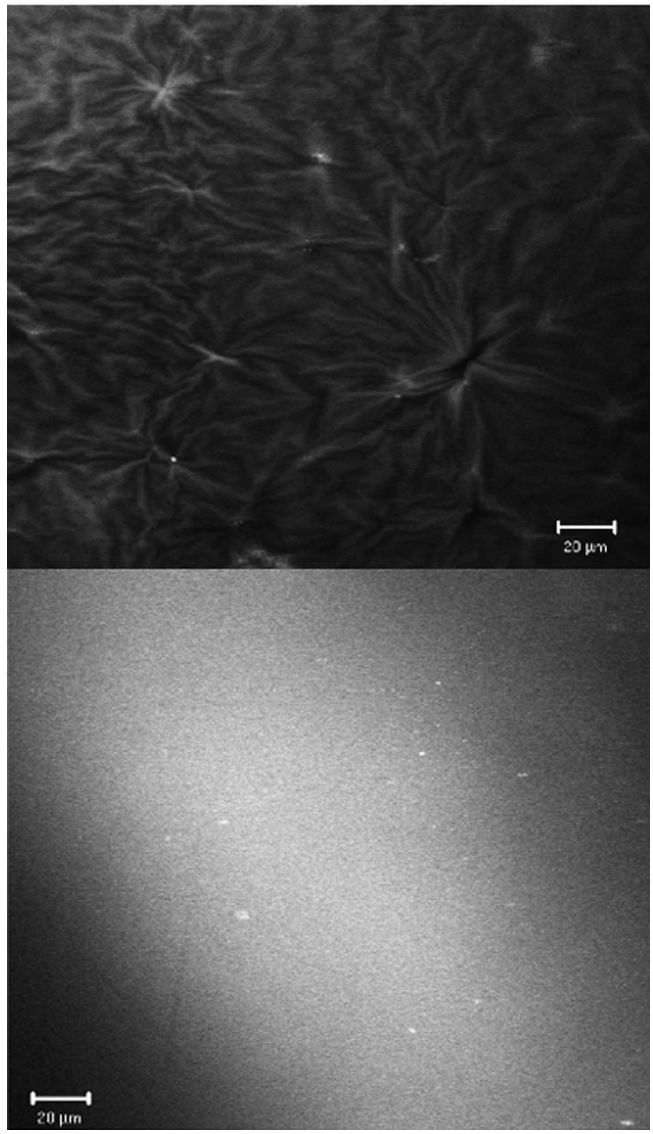

Figure 9. Left: optical micrograph, obtained by CLSM of a (PLL-HA)$_{30}$-PLL(FITC) PEM put in contact with a P_8W_{48} solution at 1.2×10^{-4} mol L^{-1} during 2 h. Right: the same architecture but without P_8W_{48}. The scale bars represent 20 μm.

In addition we found that no desorption of the P_8W_{48} occurred when they were incorporated according to method II (Figure 5 of the Supporting Information). Therefore, we have to discuss the mechanism of irreversible POM incorporation in these exponentially growing PEM films which can display an extrinsic charge compensation.[41] This means that the electroneutrality of the film is ensured by counterions. We have demonstrated in a previous study that HA-PLL films are permeable to ferrycianide anions and that this irreversible permeation is due to an anion ex-

change process.[42] We believe that the same mechanism is at the origin of the irreversible incorporation of P_8W_{48} in the same PEM architecture.

Conclusions

In this article we demonstrated that very high loading of polyoxometallates can be reached in as-built exponentially growing PEM films by putting these films in contact with a P_8W_{48} solution at different concentrations. The permeation kinetics of P_8W_{48} in the PEM film is pretty slow but the final loading efficiency is comparable to that obtained by regular LBL deposition according to method I using a POM solution at the same concentration. The advantage of loading method II is that for films having a thickness of about 1 μm, the total load of POMs can be greatly increased with respect to the traditional LBL deposition method in a single one-step process as soon as the PEM film is deposited. The response of the PEM film with respect to its swelling upon the incorporation of nanoparticles, a phenomenon already observed in a previous investigation with CdTe nanoparticles,[33] remains to be fully investigated before considering possible applications of POM containing exponentially growing PEM films. It appears also that the amount of POM loaded in the film is a non-monotonous function of the POM concentration probably in relation with the ability of the PEM film to swell in response to the incoming nanoparticles.

Experimental Section

Chemicals: $Na_{33}[H_7P_8W_{48}O_{184}]\cdot 92H_2O$ was prepared from a mixed K-Li salt (synthesized according to the literature[38]) by ion exchange to replace the counter cations by Na^+. The polyelectrolytes used to build the polyelectrolyte multilayers (PEMs) were sodium hyaluronate (HA, viscosimetric molecular weight $MW_{vis} = 4.2\times10^5$ g mol^{-1}, LifecoreBiomedical, Chaska, MN, USA) as the polyanion and poly-L-lysine (PLL, $MW_{vis} = 4.8\times10^4$ g mol^{-1}, Sigma–Aldrich, St. Louis, MA, USA, ref. P2636) as the polycation (the counteranion being Br^-). Before building films, the deposition of an anchoring layer of poly(ethylene imine) (PEI, MW = 7.5×10^5 g mol^{-1}, Sigma–Aldrich, no. P3143) was necessary for the deposition of PEM films on the amorphous carbon electrodes as well as on the ZnSe crystal used for infrared spectroscopy. The PEI layer was not necessary for film deposition on silicon oxide and quartz slides, but we nevertheless deposited such a layer to have a uniform surface treatment in our study.

All solutions were freshly prepared before use from water with a resistivity of 182 kΩ m purified in a Milli Q Plus water purification system (Millipore, Billerica, MA, USA). Two kinds of supporting electrolyte and buffer solutions were used: (i) 0.15 M NaCl solutions, without further pH adjustment, ie at pH 5.6–6.0, to dissolve PEI, HA and PLL in order to build the PEI-(HA-PLL)$_n$-HA films and (ii) 10 mM sodium acetate + 0.15 M NaCl buffer at pH 4.0 in order to build up the PEI-(P_8W_{48}-PLL)$_n$ films as well as to load the POM in PEI-(HA-PLL)$_n$-HA films. This buffer was used in order to avoid decomposition of P_8W_{48}.

PLL was conjugated with fluoresceine isothiocyanate (FITC) in order to observe the (PLL-HA)$_n$ films by confocal laser scanning microscopy. Briefly, a PLL solution at 0.7 g L^{-1} in Tris buffer (50 mM, pH 8.5) was put in contact during 1 h at ambient temperature and in the dark with FITC dissolved in a small volume of dimethyl sulfoxyde (SdS, Peypin, France). The initial ratio between the number of FITC molecules and the number of PLL monomers was lower than 10^{-5}. The PLL-FITC/free FITC mixture was then dialysed against Tris buffer solutions using a dialysis bag made of cellulose ester with a molecular weight cut-off of 10 kg mol^{-1} (Spectra/Por, Spectrum Laboratories, Rancho Dominguez, CA, USA). This dialysis step was repeated at least 2 times and was stopped when no FITC could be detected anymore in the dialysate. This was checked by UV/Vis spectroscopy at a wavelength of 494 nm.

Preparation of the PEM Films: The substrates used for ellipsometry, UV/vis experiments and confocal laser scanning microscopy (CLSM) were oxidized silicon slides (cut in 4×1 cm^2 rectangles, Siltronix, Archamps, France), quartz slides (Thuet, Blodelsheim, France) and 14 mm diameter glass slides (VWR, Fontenay-sous-bois, France), respectively. They were all cleaned in the same way by immersing them during 20 min in a piranha solution (H_2SO_4 and 30% H_2O_2 mixed in a 2:1 relation v/v) followed by extensive rinse with water.

The QCM-D experiments were performed on silica coated quartz crystals (Q Sense AB, Göteborg, Sweden), which were cleaned in situ with a 2% v/v Hellmanex solution (Hellma GmbH, Müllheim, Germany) during 30 min, rinsed with distilled water, put in contact with HCl at 0.1 M (Sigma–Aldrich) during 10 min, intensively rinsed with water, and finally with sodium acetate buffer.

The PEM films used for the loading method I, were all prepared in the same manner by putting the substrate alternatively in contact with a polycation solution (PEI at 1 g L^{-1} as the starting layer or PLL at 0.7 g L^{-1} for the following polycationic layers), buffer, a P_8W_{48} solution at 2.4×10^{-5} mol L^{-1}, and finally buffer. Each immersion lasted for 5 min. This cycle of depositions constitutes a "layer pair" and was repeated n times. In case of method II, the PEI-(HA-PLL)$_9$-HA films were deposited manually as for method I, when the loading with P_8W_{48} was investigated by means of UV/Vis and cyclic voltammetry. For CLSM experiments, we used a dipping machine (DR3, Riegler and Kirstein GmbH, Berlin, Germany) to deposit the (PLL-HA)$_{30}$ film on glass slides. The final PLL(FITC) layer was deposited manually. In these experiments each deposition step lasted for 8 min.

Characterization Methods

QCM-D: In order to define the adsorption time needed to reach saturation in the adsorbed amounts of both P_8W_{48} and PLL, the adsorption kinetics were followed using QCM-D (D300 apparatus, Q-Sense AB, Göteborg, Sweden). The working principle of this device relies on the piezoelectric properties of quartz and has been extensively described previously.[39] In the case of the Q-Sense D300 device, the oscillations of the quartz crystal are excited close to its resonance frequency of about 5 MHz. When the exciting signal is stopped, the decay of the shear wave is followed as a function of time at the fundamental frequency as well as at its 3rd, 5th and 7th overtones. From this decay curve, the pseudo frequency and the dissipation, i.e. the energy loss of the crystal in contact with the deposit and the viscous fluid are calculated as a function of time. The change in the reduced resonance frequency with respect to time will be denoted $\Delta f_n/n$ where n is the overtone number (n = 1, 3, 5 or 7). When the reduced frequency changes associated with the different harmonics overlap, the film can be considered as rigid and one can use the Sauerbrey relationship to calculate the surface coverage from the measured $\Delta f_n/n$.[34]

Ellipsometry: The thickness of the silicon oxide layer covering the silicon substrate was measured before the build up of the PEM film by ellipsometry (HORIBA Jobin Yvon, model PZ 2000, Longjumeau, France) at a wavelength of 632.8 nm and an incidence angle of 70°. The total thickness of the oxide layer and the PEM was calculated from the measured ψ and Δ ellipsometric angles assuming the film to be uniform and isotropic and using a refractive index value of 1.465 as for the silicon oxide layer (which maybe a somewhat arbitrary value owing to the fact that the PEM film contains highly refractive tungstates). The thickness values given are the average (± one standard deviation) over 5 to 10 independent measurements taken along the major axis of the rectangular silicon slide. The thickness of the PEI-(P_8W_{48}-PLL)$_n$ PEM was determined by subtracting the thickness of the SiO_2 layer from the measured total thickness. Owing to the fact that the refractive index of the film should be higher than the used value, the film thickness may be overestimated. Its geometric thickness was hence determined by means of AFM.

UV/Vis Spectroscopy: the absorption spectra were measured with a double beam mc^2 spectrophotometer (Safas, Monaco). For the determination of the extinction coefficient of P_8W_{48}, the spectra of different POM solutions in 10 mM sodium acetate + 0.15 M NaCl buffer (pH 4) were acquired in quartz cuvettes between 200 and 700 nm. The spectra of the PEI-(P_8W_{48}-PLL)$_n$ films as well as those of the PEI-(HA-PLL)$_9$-HA films after contact with P_8W_{48} containing acetate buffer were taken with the films adsorbed on quartz slides. The spectrum of the cleaned and uncoated slide was taken as the reference spectrum.

Cyclic Voltammetry: We used a conventional three electrode setup (CHI 604B, CH Instruments, Austin, TX, USA) comprising an Ag/AgCl (sat KCl) reference electrode (CHI 111), a platinum wire as a counter electrode (CHI 115) and an amorphous carbon working electrode (CHI 104). The working electrode was polished on gamma alumina powder, 0.05 μm in diameter (Buehler, Lake Bluff, IL, USA, no. 40-6325-008). Three successive polishing steps were performed, each one separated from the next one by intensive rinsing with water. The electrodes were sonicated during 6 min in a water bath just before the beginning of the electrochemical experiment. The quality of the polishing was evaluated by measuring the CV of $K_4Fe(CN)_6$ (Sigma–Aldrich, no. P9387) at 1 mM in presence of the sodium acetate buffer at pH 4.0. The electrode was used only when the difference in the oxidation and reduction potentials was between 60 and 70 mV. In case of loading method I, the CV of the deposit was acquired at different scan rates (from 10 to 200 mV s^{-1}) in the potential range between –0.9 and +0.6 V (vs. Ag/AgCl) after the deposition of each P_8W_{48} layer. Before each measurement, the buffer solution was deoxigenated by means of nitrogen bubbling during 10 min. In the case of loading method II, the CV (in the same potential range as previously) of the PEI-(HA-PLL)$_9$-HA film was taken as the reference capacitive current. The CV of the film was measured after given contact times with the P_8W_{48} containing buffer. Before each measurement, the electrode was rinsed with sodium acetate buffer and the CV was measured at different scan rates (from 10 to 200 mV s^{-1}) in the presence of deoxygenated buffer without of P_8W_{48}. Hence only the contribution of the POM present in the film to the faradaic current will be measured. The reported currents have been corrected for the capacitive currents.

Atomic Force Microscopy: AFM topographies of PEI-(P_8W_{48}-PLL)$_4$ films deposited on a QCM-D silica coated quartz crystal were acquired in the dry state and in contact mode using a Nanoscope IV (Veeco, Santa Barbara, CA, USA) microscope. The employed cantilevers (model MSCT, Veeco) had a nominative spring constant of 0.01 N m^{-1} and were terminated with a silicon nitride tip.

Infrared Spectroscopy in the Attenuated Total Reflection Mode: The details of the experimental procedure as well as the theoretical background have been reported in previous publications.[43] We used an Equinox 55 spectrometer (Bruker, Wissembourg, France) fitted with a flow cell whose bottom surface was a trapezoidal ZnSe crystal onto which the PEI-(HA-PLL)$_{12}$-HA film was deposited. Spectra were acquired after the deposition of each layer to follow the film build up. For these experiments the polyelectrolytes as well as the P_8W_{48} and its counterions were dissolved in the same buffer as for the other experiments but H_2O was replaced by D_2O (99 D atom-%, Aldrich ref. 435767) in order to avoid the interference of the water elongation bands in the spectral region between 1500–1700 cm^{-1} with the amide I and II bands of PLL. After the deposition of the PEI-(HA-PLL)$_{12}$-HA film (from a 0.15 M NaCl solution) it was rinsed with sodium acetate buffer at pD 4.4 (there is a 0.4 pH unit difference between H_2O and D_2O-containing buffers) and put in contact with the buffer containing P_8W_{48} at a given concentration. This solution was allowed to flow atop the film during 2 h, the film was rinsed with buffer and the spectrum was measured. The absorbance was calculated by taking the transmission through the PEI-(HA-PLL)$_{12}$-HA film as the reference.

Confocal Laser Scanning Microscopy (CLSM): The (PLL-HA)$_{30}$-PLL(FITC) films were imaged with an LSM 510 inverted confocal laser scanning microscope (Zeiss, Oberkochen, Germany). The cover glasses supporting the PEM films were placed in a homemade sample holder in 10 mM sodium acetate plus 0.15 M NaCl buffer (pH 4.0). The FITC molecules were excited at a wavelength of 488 nm with a 25 mW argon ion laser and the emitted fluorescence was collected at wavelengths between 505 nm and 530 nm. The employed immersion objective (Plan Neofluar, Zeiss) had a 40-times magnification and a numerical aperture of 1.3. Stacks of line scans with a length of 230.3 μm in the sample plane were acquired at a resolution of 512 pixels and combined to virtual *z*-sections to measure the film thickness at five different places of each sample. The number of line scans and their distance normal to the sample plane were calculated by the operating software of the microscope as a function of the sample thickness. The film was imaged before being in contact with the POM solutions as well as after 2 h of contact and rinsing with the acetate/NaCl buffer. The ratio between the film thickness after loading with P_8W_{48} and its initial thickness allowed calculating the relative film thickness.

Supporting Information (see also the footnote on the first page of this article): Evolution of the PEI-(P_8W_{48}-PLL)$_n$ film thickness measured by ellipsometry as a function of the number of deposited layer pairs, cyclic voltammograms and oxidation currents corresponding to peak A1 of a PEI-(P_8W_{48}-PLL)$_4$ film as a function of the potential scan rate, ATR FTIR spectra showing the buildup of PEI-(HA-PLL)$_n$ films as a function of n, relative thickness measured by CLSM of (PLL-HA)$_{30}$-PLL(FITC) films after 2 h of contact with P_8W_{48} solutions at different concentrations, evolution of the UV/Vis spectrum of a PEI-(HA-PLL)$_9$-HA film loaded with P_8W_{48} (at 1.2×10^{-5} mol L^{-1} during 1 h) and put in sodium acetate buffer (pH 4) during 10 h.

Acknowledgments

We thank Cosette Betscha for her help with the ATR-FTIR experiments.

[1] J. Berzelius, *Poggendorff's Ann. Phys.* **1826**, *6*, 369–374.

[2] a) J. F. Keggin, *Nature* **1933**, *131*, 908–909; b) M. T. Pope, *Heteropoly and Isopoly Oxometalates*, Springer, Berlin, **1983**; c) M. T. Pope, A. Müller, *Angew. Chem. Int. Ed. Engl.* **1991**, *30*, 34–48.
[3] A. Müller, S. Roy, *Oxomolybdates: From Structures to Functions in a new area of Nanochemistry*, in: *The Chemistry of Nanomaterials, Synthesis Properties and Applications*, vol. 2 (Eds.: C. N. R. Rao, A. Müller, A. K. Cheetham), Wiley-VCH, Weinheim, Germany, **2004**.
[4] C. L. Hill, C. M. Prosser-McCartha, *Coord. Chem. Rev.* **1995**, *143*, 407–455.
[5] T. Yamase, *Chem. Rev.* **1998**, *98*, 307–326.
[6] J. T. Rhule, C. L. Hill, D. A. Judd, R. F. Shinazi, *Chem. Rev.* **1998**, *98*, 327–358.
[7] B. Hasenknopf, *Front. Biosci.* **2005**, *10*, 275–287.
[8] X. Wang, J. Liu, M. T. Pope, *Dalton Trans.* **2003**, 957–960.
[9] X. Wang, J. Liu, J. Li, Y. Yang, J. Liu, B. Li, M. T. Pope, *J. Inorg. Biochem.* **2003**, *94*, 279–284.
[10] C. L. Hill, M. S. Weeks, R. F. Shinazi, *J. Med. Chem.* **1990**, *33*, 2767–2772.
[11] W. G. Klemperer, C. G. Wall, *Chem. Rev.* **1998**, *98*, 297–306.
[12] M. Clemente-Leon, C. Mingotaud, B. Agricole, C. J. Gomez-Garcia, E. Coronado, P. Delhaes, *Angew. Chem. Int. Ed. Engl.* **1997**, *36*, 1114–1116.
[13] D. Ingersoll, P. J. Kulesza, L. F. Faulkner, *J. Electrochem. Soc.* **1994**, *141*, 140–147.
[14] G. Decher, *Science* **1997**, *277*, 1232–1237.
[15] a) N. G. Hoogeveen, M. A. Cohen Stuart, G. J. Fleer, M. R. Böhmer, *Langmuir* **1996**, *12*, 3675–3681; b) G. Ladam, P. Schaad, J.-C. Voegel, P. Schaaf, G. Decher, F. J. G. Cuisinier, *Langmuir* **2000**, *16*, 1249–1255.
[16] E. Donath, G. B. Sukhorukov, F. Caruso, S. A. Davis, H. Möhwald, *Angew. Chem. Int. Ed.* **1998**, *37*, 2201–2205.
[17] a) J. B. Schlenoff, S. T. Dubas, T. R. Fahrat, *Langmuir* **2000**, *16*, 9968–9969; b) A. Izquierdo, S. S. Ono, J.-C. Voegel, P. Schaaf, G. Decher, *Langmuir* **2005**, *21*, 7558–7567; c) C. Porcel, Ph. Lavalle, V. Ball, G. Decher, B. Senger, J.-C. Voegel, P. Schaaf, *Langmuir* **2006**, *22*, 4376–4383.
[18] a) P. A. Chiarelli, M. S. Johal, J. L. Casson, J. B. Roberts, J. M. Robinson, H.-L. Wang, *Adv. Mater.* **2001**, *13*, 1167–1171; b) C. Jiang, S. Markutsia, V. V. Tsukruk, *Adv. Mater.* **2004**, *16*, 157–161.
[19] a) K. Ariga, J. P. Hill, Q. Ji, *Phys. Chem. Chem. Phys.* **2007**, *9*, 2319–2340; b) K. Ariga, J. P. Hill, M. V. Lee, A. Vinu, R. Charvet, S. Acharya *Sci. Tech. Adv. Mater* **2008**, 9, art014109.
[20] Z. Tang, Y. Wang, P. Podsiadlo, N. A. Kotov, *Adv. Mater.* **2006**, *18*, 3203–3224.
[21] a) Y. Wang, A. S. Angelatos, F. Caruso, *Chem. Mater.* **2008**, *20*, 848–858; b) B. G. De Geest, N. N. Sanders, G. B. Sukhorukov, J. Demeester, S. C. De Smet, *Chem. Soc. Rev.* **2007**, *36*, 636–649.
[22] I. Ichinose, H. Tagawa, S. Mizuki, Y. Lvov, T. Kunitake, *Langmuir* **1998**, *14*, 187–192.
[23] a) F. Caruso, D. G. Kurth, D. Volkmer, M. J. Koop, A. Müller, *Langmuir* **1988**, *14*, 3462–3465; b) D. G. Kurth, D. Volkmer, M. Ruttorf, B. Richter, A. Müller, *Chem. Mater.* **2000**, *12*, 2829–2831; c) S. Liu, D. G. Kurth, D. Volkmer, *Chem. Commun.* **2002**, 976–977; d) S. Liu, D. G. Kurth, B. Bredenkötter, D. Volkmer, *J. Am. Chem. Soc.* **2002**, *124*, 12279–12287; e) S. Liu, H. Möhwald, D. Volkmer, D. G. Kurth, *Langmuir* **2006**, *22*, 1949–1951.
[24] L. Cheng, J. A. Cox, *Electrochem. Commun.* **2001**, *3*, 285–289.
[25] Y. Wang, C. Guo, Y. Chen, C. Hu, W. Yu, *J. Colloid Interface Sci.* **2003**, *264*, 176–183.
[26] L. Wang, J. Li, E. B. Wang, L. Xu, J. Peng, Z. Li, *Mater. Lett.* **2004**, *58*, 2027–2031.
[27] Y. Feng, Z. Han, J. Peng, J. Lu, B. Xue, L. Li, H. Ma, E. Wang, *Mater. Lett.* **2006**, *60*, 1588–1593.
[28] C. Li, K. P. O'Halloran, H. Ma, S. Shi *J. Phys. Chem. B* **2009**, published as ASAP article.
[29] D. Jabbour, B. Keita, L. Nadjo, U. Kortz, S. Sankar Mal, *Electrochem. Commun.* **2005**, *7*, 841–847.
[30] a) T. R. Fahrat, J. B. Schlenoff, *Langmuir* **2001**, *17*, 1184–1192; b) T. R. Fahrat, J. B. Schlenoff, *J. Am. Chem. Soc.* **2003**, *125*, 4627–4636; c) S. Han, B. Lindholm-Sethson, *Electrochim. Acta* **1999**, *45*, 845–853.
[31] a) C. Picart, Ph. Lavalle, P. Hubert, F. J. G. Cuisinier, G. Decher, P. Schaaf, J.-C. Voegel, *Langmuir* **2001**, *17*, 7414–7424; b) C. Picart, J. Mutterer, L. Richert, Y. Luo, G. D. Prestwich, P. Schaaf, J.-C. Voegel, Ph. Lavalle, *Proc. Natl. Acad. Sci. USA* **2002**, *99*, 12531–12535; c) F. Boulmedais, V. Ball, P. Schwinte, B. Frisch, P. Schaaf, J.-C. Voegel, *Langmuir* **2003**, *19*, 440–445.
[32] E. Hübsch, G. Fleith, J. Fatisson, P. Labbé, J.-C. Voegel, P. Schaaf, V. Ball, *Langmuir* **2005**, *21*, 3664–3669.
[33] S. Srivastava, V. Ball, P. Podsiadlo, J. Lee, P. Ho, N. A. Kotov, *J. Am. Chem. Soc.* **2008**, *130*, 3748–3749.
[34] G. Sauerbrey, *Z. Phys.* **1959**, *155*, 206–222.
[35] S. Sankar Mal, U. Kortz, *Angew. Chem. Int. Ed.* **2005**, *44*, 3777–3780.
[36] F. Höök, J. Vörös, M. Rodahl, R. Kurrat, P. Böni, J. J. Ramsden, M. Textor, N. D. Spencer, P. Tengvall, J. Gold, B. Kasemo, *Colloids Surf. B* **2002**, *24*, 155–170.
[37] A. P. Brown, F. C. Anson, *Anal. Chem.* **1977**, *49*, 1589–1595.
[38] R. Contant, A. Tézé, *Inorg. Chem.* **1985**, *24*, 4610–4614.
[39] M. V. Voinova, M. Rodahl, M. Jonson, B. Kasemo, *Phys. Scr.* **1999**, *59*, 391–399.
[40] D. Collin, Ph. Lavalle, J. Mendez-Garza, J.-C. Voegel, P. Schaaf, Ph. Martinoty, *Macromolecules* **2004**, *37*, 10195–10198.
[41] J. B. Schlenoff, H. Ly, M. Li, *J. Am. Chem. Soc.* **1998**, *120*, 7626.
[42] V. Ball, E. Hübsch, R. Schweiss, J.-C. Voegel, P. Schaaf, W. Knoll, *Langmuir* **2005**, *21*, 8526–8531.
[43] V. Ball, F. Bernsmann, C. Betscha, C. Maechling, S. Kauffmann, B. Senger, J.-C. Voegel, P. Schaaf, N. Benkirane-Jessel, *Langmuir* **2009**, *25*, 3593–3600.

Received: June 30, 2009
Published Online: September 1, 2009

